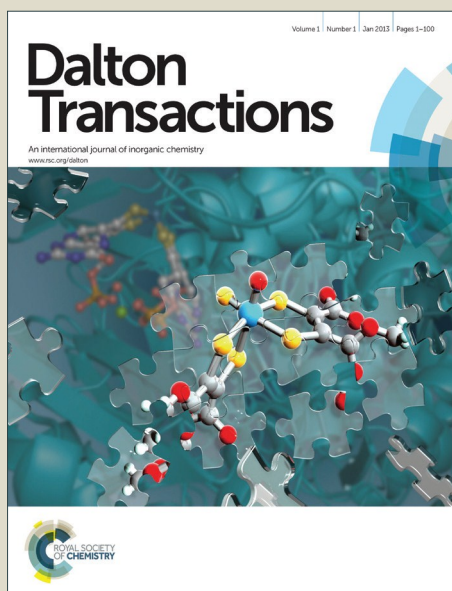


Dalton Transactions

Accepted Manuscript



This article can be cited before page numbers have been issued, to do this please use: L. Tesi, A. Lunghi, M. Atzori, E. Lucaccini, L. Sorace, F. Totti and R. Sessoli, *Dalton Trans.*, 2016, DOI: 10.1039/C6DT02559E.



This is an *Accepted Manuscript*, which has been through the Royal Society of Chemistry peer review process and has been accepted for publication.

Accepted Manuscripts are published online shortly after acceptance, before technical editing, formatting and proof reading. Using this free service, authors can make their results available to the community, in citable form, before we publish the edited article. We will replace this *Accepted Manuscript* with the edited and formatted *Advance Article* as soon as it is available.

You can find more information about *Accepted Manuscripts* in the [Information for Authors](#).

Please note that technical editing may introduce minor changes to the text and/or graphics, which may alter content. The journal's standard [Terms & Conditions](#) and the [Ethical guidelines](#) still apply. In no event shall the Royal Society of Chemistry be held responsible for any errors or omissions in this *Accepted Manuscript* or any consequences arising from the use of any information it contains.

Giant spin-phonon bottleneck effects in evaporable vanadyl-based molecules with long spin coherence

L. Tesi,^a A. Lunghi,^{a,b} M. Atzori,^a E. Lucaccini,^a L. Sorace,^a F. Totti,^a and R. Sessoli^{a,*}

Received 00th January 20xx,
Accepted 00th January 20xx

DOI: 10.1039/x0xx00000x

www.rsc.org/

Vanadium(IV) complexes have recently shown record quantum spin coherence times that in several circumstances are limited by spin-lattice relaxation. The role of the environment and vibronic properties in the low temperature dynamics is here investigated by a comparative study of the magnetization dynamics as a function of crystallites size and steric hindrance of the β -diketonate ligands in VO(acac)₂ (**1**), VO(dpm)₂ (**2**) and VO(dbm)₂ (**3**) evaporable complexes (acac⁻ = acetylacetonate, dpm⁻ = dipivaloylmethanate, and dbm⁻ = dibenzoylmethanate). A pronounced crystallites size dependence of the relaxation time is observed at unusually high temperatures (up to 40 K) which is associated to a giant spin-phonon bottleneck effect. We model this behaviour by an ad-hoc force field approach derived from density functional theory calculations, which evidences a correlation of the intensity of the phenomenon with ligand dimensions and unit cell size.

Introduction

Magnetic molecules characterized by a large spin and easy axis magnetic anisotropy have been the focus of significant interest since two decades.¹ The interest in their properties is dual: from one side, their long relaxation time of the magnetization makes them appealing to build miniaturized memory units, while, from a fundamental point of view, they are studied as model systems to investigate quantum effects in the magnetization dynamics. Molecular magnets are nowadays investigated also at single molecule level mainly depositing them on surfaces^{2,3} or inside nanojunctions⁴ to realize single molecule spintronics devices.^{5,6} More recently another class of magnetic molecules, characterized by a small ($S=1/2$) and essentially isotropic spin state gained much attention thanks to their relatively long spin-spin or spin coherence time, T_2 .⁷⁻¹⁴ The latter is one of the key features if a system has to be used as a quantum bits, or qubits, *i.e.* the fundamental unit of a quantum computer.¹⁵ Though many different physical realizations of qubits are available, magnetic molecules present some advantages. First, the electronic spin is the most intuitive and simple choice to reproduce the sought-after quantum behaviour of qubits¹⁵. Moreover, molecules can be

processed to obtain ordered nanostructures, which is a prerequisite if a real device is to be developed,¹⁰ and synthetic chemistry techniques allow in principle to tune the interaction to couple two or more qubits.^{16,17} On the other hand, their spin coherence time (*i.e.* the lifetime of any quantum superposition of states), is, in general, significantly shorter than that observed for other qubits candidates based on electronic spins, such as defects in inorganic semiconductors.^{18,19} However, remarkably long quantum coherence times have been recently achieved in molecular systems by a rational design of the nuclear spin environment. Freedman *et al.*¹⁴ reported on a value of the phase memory time T_m (a lower estimation of T_2), for a vanadium(IV) complex dissolved in CS₂ of ca. 0.7 ms at 10 K. Furthermore, dilution in crystalline matrices provided detectable quantum coherence at room temperature in [(Ph)₄P]₂[Cu(mnt)₂] (mnt = maleonitriledithiolate)⁸ and, more recently, for the processable VOPc (Pc = phthalocyanine) complex, where Rabi oscillations were also observed at room temperature.⁹ Although the optimization of quantum coherence times is fundamental to perform coherent quantum logic operations, another step toward the integration of these molecular systems in real devices is their controlled deposition on solid surfaces and the investigation of their quantum coherence in the hybrid architecture. In this respect, still very little is known about the role that unusual environment, such as that of an isolated molecule on a surface, can have on spin lattice relaxation time, T_1 , as well as on T_2 . Indeed, a recent report highlighted the environment role played by a substrate made of a thin layer of MgO deposited on Ag on the magnetic

^a Dipartimento di Chimica "Ugo Schiff" e INSTM, Università degli Studi di Firenze, Via della Lastruccia 3, I50019 Sesto Fiorentino (Firenze), Italy

^b School of Physics, CRANN and AMBER Trinity College Dublin 2, Ireland.

Electronic Supplementary Information (ESI) available: X-ray powder diffraction data, EPR spectra and analysis, AC susceptibility data, and details on the Force Field and DFT calculations. See DOI: 10.1039/x0xx00000x

bistability of a Ho atom, which reaches a very long relaxation time for the magnetization, 1500 s at 10 K.²⁰

We have recently shown that the combination of alternating current (AC) susceptometry and pulsed electron paramagnetic resonance (EPR) spectroscopy can help to identify molecular systems with long-lived coherence at high temperature, where the coherence time is limited by the spin-lattice relaxation.⁹ In our previous studies,¹⁰ we observed relatively long T_m for frozen solutions of VO(dpm)₂ (dpm⁻ = dipivaloylmethanate), 2 μs at 80 K, and an anomalous coefficient for the direct mechanism of spin-lattice relaxation at low temperatures. The latter behaviour was attributed to the spin-phonon bottleneck effect, a phenomenon due to the lack of an efficient exchange between spins and the thermal bath mediated by low-frequency phonons, with the resulting slowing down of the relaxation process.²¹ This environmental effect, that depends on the crystallites size and on the concentration of paramagnetic ions, is particularly relevant for $S=1/2$ systems at low temperature, when the relaxation occurs through the direct process, which involves low energy resonant phonons.²²⁻²⁵ On the contrary few observations²⁶⁻²⁸ on spin-phonon bottleneck effects were reported for molecules with spin higher than 1/2, e.g. Single Molecule Magnets (SMMs), because multi-phonon processes like the Orbach mechanism, which involves higher energy phonons, dominate.¹

The interaction of the magnetic systems with the environment presents several crucial aspects which involves structural, electronic, and vibrational properties. In this framework, the spin-phonon bottleneck effect in molecular systems is an intriguing issue that can evidence the key role of the environment on the magnetic relaxation and consequently also on the quantum coherence time. Indeed, it is clear that a deeper understanding of this effect and its control by tiny chemical modifications could in principle allow a further enhancement of the quantum coherence time.

To evaluate the spin-phonon bottleneck effect in potential molecular spin qubits, we have performed an experimental investigation of the spin dynamics of the magnetization for three crystalline vanadyl β-diketonate complexes, namely VO(acac)₂ (**1**), VO(dpm)₂ (**2**) and VO(dbm)₂ (**3**) (acac⁻ = acetylacetonate, dpm⁻ = dipivaloylmethanate, and dbm⁻ = dibenzoylmethanate), which feature the same vanadyl ion and ligand moiety with substituents of different steric hindrance. The spin dynamics of compounds **1-3** have been investigated by AC susceptometry on macro and microcrystalline samples over a wide range of temperatures and static magnetic fields. A giant spin-phonon bottleneck effect, detectable up to 40 K, with relaxation times of the magnetization, τ , spanning two orders of magnitude depending on the crystallite sizes, has been observed. Theoretical modelling has been used to get insights on the origin of this effect. For that purpose, an ad-hoc force field for the three systems has been derived from density functional theory (DFT) calculations and exploited to rationalize lattice properties such as phonon dispersion curves and vibrational density of states (DOS) for the three complexes. A strong correlation of the intensity of the

phenomenon with ligand dimensions and unit cell size has been evidenced.

DOI: 10.1039/C6DT02559E

Results and discussion

Synthesis and crystal structures description

1, **2** and **3** were prepared according to a general synthetic procedure already reported in the literature.²⁹ The reaction between an aqueous solution of VOSO₄·xH₂O and the β-diketonate ligand (1:2 molar ratio) partially deprotonated with Na₂CO₃ in EtOH/H₂O (1:1) solution affords the desired products in good yields. Polycrystalline samples of compounds **1-3** were characterized through powder X-ray diffraction (PXRD) analyses by comparing the experimental patterns with those calculated from the atomic coordinates of the reported single crystal X-ray structures.³⁰⁻³² The good agreement between experimental and simulated patterns (see ESI, Figures S1-S3) demonstrates the phase purity of the investigated samples.

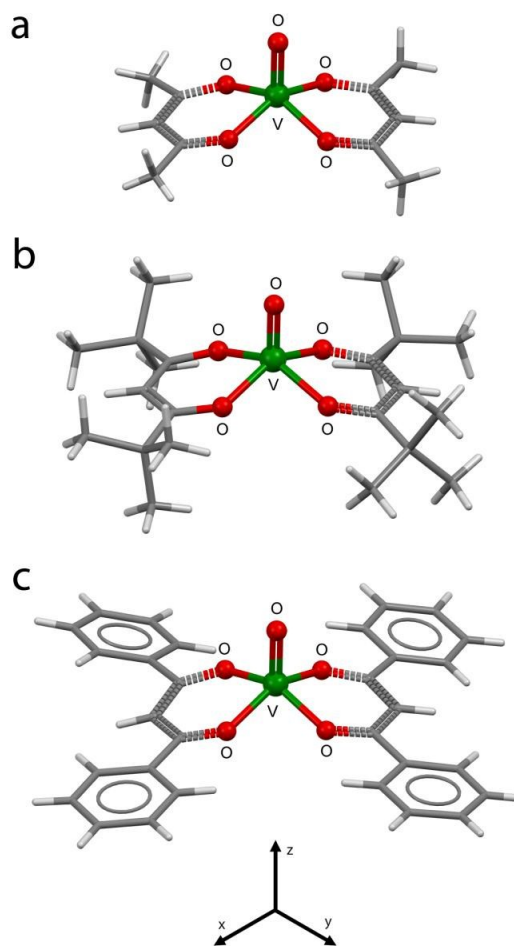


Figure 1. Molecular structures of **1** (a), **2** (b), and **3** (c), with principal atoms labelling scheme and coordination geometry of the V^{IV} ions highlighted.

All investigated compounds show a vanadyl ion VO^{2+} coordinated by two chelating bidentate β -diketonate ligands. The coordination geometry around the penta-coordinated V^{IV} metal centre is a distorted square pyramid with the metal ion slightly above the basal plane (0.545(1) Å (**1**), 0.573(1) Å (**2**), 0.559(1) Å (**3**)) (Figure 1). The V=O bond distances are 1.585(1) Å, 1.574(1) Å, and 1.578(1) Å for **1**, **2** and **3**, respectively, whereas the average V–O bond lengths are 1.969(2) Å for **1**, 1.964(2) Å for **2**, and 1.946(2) Å for **3**. The V=O double bond, being ca. 0.4 Å shorter than the V–O single bonds, induces a strong axial distortion of the ligand field acting on the d -orbitals of the metal ion; this, together with the out of plane position of the metal atom, results in the d_{xy} orbital lying lowest and being singly occupied. The large energy difference between the magnetic orbital and the unoccupied ones make these $S = 1/2$ systems ideal candidates as molecular spin qubits.³³

The substituents on the common β -diketonate ligand moiety have a steric hindrance that increase in the order **1** < **2** < **3**. Accordingly, the unit cell parameters increase in the same order, although they are further increased by the higher symmetry of the space groups of **3**. Indeed, even if all compounds crystallize with only one crystallographically independent molecule in the asymmetric unit, **1** crystallizes in the triclinic centrosymmetric space group $P\bar{1}$ ($Z=2$), whereas **2** and **3** crystallize in the $P2_1$ and $Pbca$ monoclinic space groups with $Z = 2$ and $Z = 8$, respectively. Such crystallographic differences have important implications on the theoretical calculations of the lattice properties (*vide infra*).

The very similar coordination environment along the series is reflected in practically identical frozen solution EPR spectra (Figure S4), which show the typical features of an anisotropic doublet interacting with an $I = 7/2$ nuclear spin (^{51}V , n. ab. 99.75%). The spectra have been simulated³⁴ on the basis of the Spin Hamiltonian $\mathbf{H} = \mu_B \mathbf{B} \cdot \mathbf{g} \cdot \mathbf{S} + \mathbf{I} \cdot \mathbf{A} \cdot \mathbf{S}$, providing almost identical parameters for the three derivatives (Table S1) indicating only negligible differences in the electronic structure of the complexes. The obtained parameters are in the range previously reported for VO^{2+} β -diketonate-type derivatives^{35, 36} and are characterized, as expected, by partially rhombic \mathbf{g} and \mathbf{A} tensors. Larger deviations from the free electron values for \mathbf{g} and larger hyperfine coupling are observed along the z direction, which is directed along the V=O bond.³⁶ The corresponding field/energy levels obtained for field applied along z and along x axis are reported in Figure S5.

Magnetization dynamics

The investigation of the spin-phonon bottleneck effect was based on the comparison of AC susceptibility data measured for several samples of **1-3** made up of crystallites of different sizes. We began our investigation by measuring AC magnetic susceptibility as a function of the applied static magnetic field (Figure 2) and temperature (Figure 3a) on three polycrystalline samples of **1** with different crystallite dimensions (d): macroscopic crystals as obtained from crystallization (d ca. 1-5 mm) (**1a**), moderately crushed crystals (d ca. 500 μm) (**1b**), and well crushed and pressed microcrystalline powders (d ca. 10

μm) (**1c**). The dimensions of the crystallites were qualitatively estimated by X-ray microtomography (Figure S6). As expected, the imaginary component of magnetic susceptibility, χ'' , is zero for all the compounds in zero static magnetic field; on application of a moderate static magnetic field (20 mT) a maximum in the $\chi''(\nu)$ plot is observed accompanied by a concomitant decrease of the real part, χ' (Figure S7-S9). The Debye model¹ has been used to reproduce the frequency dependence of χ'' , thus allowing to extrapolate the values of the relaxation time, τ , the width of the relaxation time distribution, α , and the difference between isothermal and adiabatic susceptibility, $\chi_T - \chi_S$ as a function of temperature and applied field.

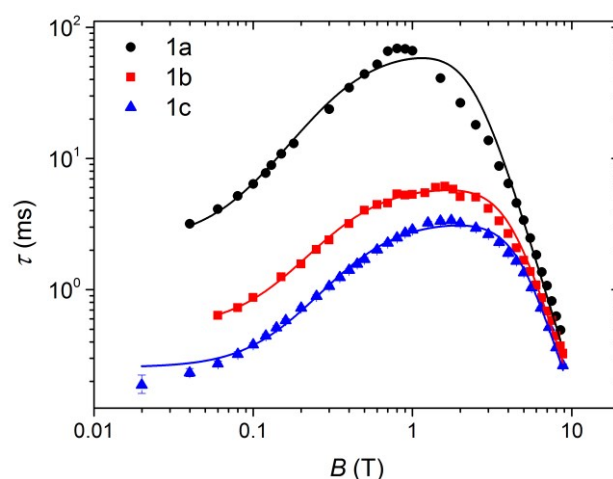


Figure 2. Magnetization relaxation time for samples **1a**, **1b**, **1c** as a function of the static magnetic field at $T = 10$ K, reported as a log-log plot. Solid lines are best fit curves obtained by using eq. (1) with the parameters reported in Table 1.

It is evident from Figure 2 that the three morphologically different samples show very different absolute values of the relaxation time τ , which is ca. one order of magnitude higher for **1a** with respect to **1c** at $T = 10$ K and B up to 1 T. Remarkably the sample dependence of τ remains constant up to 1-2 T but almost disappears at the highest investigated field of 9 T. On the other hand, it increases dramatically on lowering the temperature, being as high as two orders of magnitude at $T = 5$ K and $B = 0.2$ T (Figure 3a).

The field dependence of the relaxation time follows for all three samples a behaviour observed for other vanadyl-based compounds^{9, 10}, which can be simulated using equation (1), derived from the Brons-van Vleck model.^{37, 38}

$$\tau^{-1} = cB^4 + d \frac{1 + eB^2}{1 + fB^2} \quad (1)$$

The first term accounts for the field dependence of the direct mechanism of relaxation between two states split by the Zeeman energy, while the second term takes into account several mechanisms of mixing between the levels depending on inter and intramolecular interactions. The best-fit parameters are reported in Table 1.

The observed differences between **1a**, **1b** and **1c** could be in principle due to a non-statistical random orientation of the crystals, especially for non-crushed crystallites, as in sample **1a**: the anisotropic Spin Hamiltonian parameters might indeed result in different relaxation times for field applied along different directions. To test this hypothesis, a 5.4 mg single crystal of **1** was investigated, following the same protocol used for polycrystalline samples, by applying the static and AC magnetic fields parallel and perpendicular to the V=O bond. The triclinic space group of this derivative further assures that all molecules in the crystal structure have the same orientation of the **g** and **A** tensors, thus providing the same energy pattern for all the molecules in a given applied field. The results, reported in ESI, Figure S10, revealed no significant differences between the two orientations, clearly demonstrating the key role of the crystallites dimensions in determining the spin dynamics. Indeed, these results evidence that the strong anisotropy in the hyperfine interaction does not play a role in the investigated field and temperature range, despite that both energy and composition of the eigenstates are strongly affected by the orientation of the field (Figure S5). The reason is that at the investigated temperatures all the 16 states of the hyperfine split doublet are essentially equi-populated: temperatures below 100 mK will be necessary to evidence nuclear spin effects on the dynamics of the magnetization.³⁹

Having established that the observed differences in τ are due to the different crystallite sizes in the three samples and then to spin-phonon bottleneck effects, the reduced differences observed at higher field values (Figure 2) can be easily explained. Indeed, the splitting of the $S=1/2$ doublet increases with the field and phonons of higher frequency are involved in the resonant mechanism of relaxation, thus reducing the efficiency of the spin-phonon bottleneck effect.

Sample	$c \cdot 10^{-4} (\text{T}^{-4} \text{ms}^{-1})$	$d (\text{ms}^{-1})$	$e (\text{T}^2)$	$f (\text{T}^2)$
1a	4.8 ± 0.2	0.5 ± 0.2	11 ± 3	248 ± 163
1b	6.0 ± 0.2	1.9 ± 0.1	6.1 ± 0.6	72 ± 10
1c	6.3 ± 0.1	4.0 ± 0.3	4.2 ± 0.3	56 ± 6

Table 1. Best-fit parameters of the model (eq. 1) used to reproduce the field dependence of the magnetization relaxation rate τ^{-1} for **1a**, **1b** and **1c**.

A pronounced dependence of τ for **1** on crystallites size is also evident by analysing its temperature dependence (Figure 3a). These differences become more evident on lowering the temperature, but are still present at the highest investigated temperature, 42 K. The slopes in the log-log plot of τ for the three samples and their trends are quite different: they tend to the same value at high temperature, but from ca. 20 K to lower temperature, the slope for **1b** and **1c** decreases, while for **1a** increases. This behaviour can be qualitatively interpreted as due to two different regimes: a low temperature one, where direct process dominates, and a higher temperature one, where a Raman-like process drives the relaxation.⁴⁰ According to this interpretation, we obtained the slope coefficients under and above 20 K for **1a**, **1b** and **1c** by two distinct linear fits (Table 2) of the thermal dependence of τ .

Sample\Temperature	< 20 K	> 20 K
1a	4.2	3.4
1b	1.9	2.7
1c	1.5	2.4

Table 2. Slopes of the temperature dependence of τ in the log-log plot for **1a**, **1b**, and **1c**, given as the n parameter of $\tau \propto T^n$.

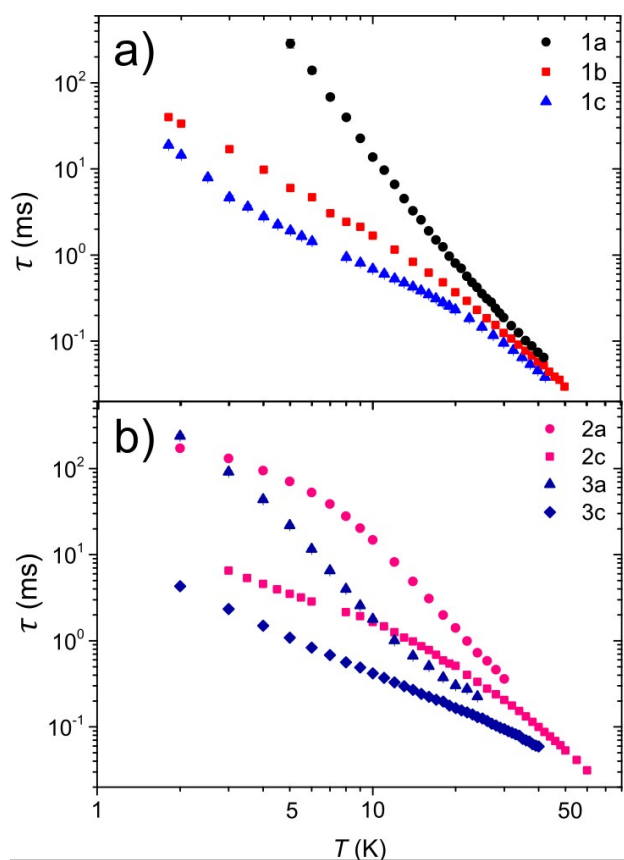


Figure 3. Temperature dependence of the magnetization relaxation time for **1a**, **1b** and **1c** (a) and for **2a**, **2c** and **3a**, **3c** (b), at $B = 0.2$ T.

The results reported in Table 2 are unusual because the direct mechanism, which is dominant at low temperature, should depend linearly on temperature, while deviations from this behaviour are observed for all samples, especially for **1a**. Above 20 K the Raman-like mechanism dominates and a T^{-3} dependence on temperature, typical of vanadyl-based systems^{9, 10, 41, 42}, is observed.

To describe the paramagnetic relaxation in presence of the spin-phonon bottleneck effect Stoneham²³ derived, from thermodynamic bases, an equation to take into account the contributions involved in the relaxation (equation 2), independently from the mechanisms of the relaxation process:

$$\tau = \tau_{SL} + \left(\frac{c_S}{c_L}\right) \tau_{LB} \quad (2)$$

where τ is the spin-bath relaxation time, actually the one measured by AC susceptibility, τ_{SL} is the spin-lattice relaxation time, c_S is the specific heat of the spin system, c_L the lattice specific heat, and τ_{LB} the lattice-bath relaxation time. Equation (2) suggests that, if τ_{LB} is high enough, a variation of the magnetic ions concentration (equal to a change in c_S/c_L) or on the crystallite size (equal to a change of τ_{LB}) results in a modification of the observed relaxation time.

The rate-determining step for the phonon-bath exchange process could involve the transfer of energy in space (spatial bottleneck) or in frequency (spectral bottleneck). Stoneham observed that when spatial bottleneck dominates then $\tau \rightarrow \tau_{LB} \cdot T^{-2}$ and $\tau_{LB} \propto d$, where d is the size of the crystallites. The exponent $n=2$ in $\tau \propto T^n$, originated by the specific heat ratio in eq. (2), is indeed the most commonly found in $S = 1/2$ systems affected by the spin-phonon bottleneck,²⁴ including the pseudo-spin $S=1/2$ of an Yb^{III} complex.²² However, van Vleck suggested that, taking into account the finite life time of phonons, τ_{LB} could also depend on temperature and an exponent up to $n = 6$ can be expected.²¹ The latter seems the case of **1a**, which, thanks to the rapid divergence at low temperature, reaches remarkable large values of τ , e.g. 400 ms at 5 K, and shows butterfly-like magnetic hysteresis around 2 K (Figure S11). This occurs at a much higher temperature than previously observed in other vanadium(IV) containing systems.²⁵

To confirm that our observation can be associated to a poorly efficient energy transfer to the thermal bath and not to changes induced by the mechanical stress on the crystallites, we have investigated the magnetization dynamics of **1a** covered by activated carbon (**1a'**). This is expected to favour the thermal exchange between the helium gas (acting as the bath) and the crystallites, resulting in a faster relaxation process. The extracted spin-lattice relaxation times, (Figure S12) evidence a small but significant reduction of τ for **1a'**, and that this effect is more pronounced at low temperature. These results confirm that the heat exchange between the crystallites and the bath plays a key role in determining the relaxation time.

Finally, to evaluate the contribution of the crystal and the molecular structures on spin-phonon bottleneck, we analysed the magnetization dynamics of **2** and **3**. AC susceptibility was measured only for macroscopic crystallites as obtained from crystallization (d ca. 1 mm) (**2a** and **3a**) and for the same crystallites subsequently crushed in microcrystalline powders (d ca. 10 μm) (**2c** and **3c**), in the same field and temperature range of **1**. The data for the real, χ' , and the imaginary, χ'' , component of the susceptibility for **2** and **3** are reported in the supporting information (Figure S13-S16). Figure 3b shows the temperature dependence of the extrapolated relaxation times τ , evidencing that, as observed for **1**, also **2** and **3** exhibit a significant dependence of τ on the crystallite size.

To directly compare the effect of the crystallite size on τ , and thus the relative importance of the bottleneck effect in

the three investigated complexes, we also report in Figure 4 the ratio between the relaxation time τ of the macroscopic crystallites (**a**) and that of the crushed crystallites (**c**). Indeed, according to eq. (2), in the macroscopic crystallites the effect should be maximum, whereas it should be negligible in the other one. This approach allows to highlight a clear trend for the three compounds: the smaller the mass of the molecule, the higher is the temperature at which size effects become visible. We further note that while **1** and **3** show a constant increase of this ratio on lowering the temperature, **2** reaches a plateau around 5 K. This is probably due to the different morphology of the crystals: **1** and **3** form almost isometric crystals, while **2** forms thin plates, thus hampering to reach the infinite size regime for this compound.

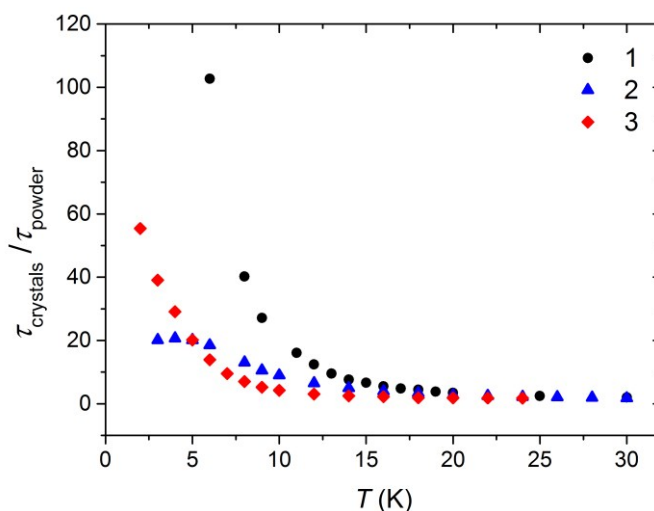


Figure 4. Ratio of the spin-lattice relaxation time between macroscopic crystallites (crystals) and crushed crystallites (powders) for **1**, **2** and **3** as a function of the temperature at $B = 0.2$ T.

We can conclude that this experimental investigation surprisingly proved a neat and remarkable relation between the dynamic magnetic properties of vanadyl β -diketonate and their organic ligands moieties, suggesting a strong correlation between the spin relaxation and vibrational degrees of freedom.

Theoretical calculations

In order to provide a microscopic link between the observed experimental behaviour for the relaxation time in **1**, **2** and **3** and their structural features, lattice dynamics simulations were performed for all of them.

The phonon dispersion curves for **1-3**, reported in Figure 5, have been calculated along the arbitrary path $X(0.5,0,0)-\Gamma(0,0,0)-Y(0,0,0.5)-\Gamma(0,0,0)-Z(0,0,0.5)$, where the coordinates are expressed in the reciprocal lattice basis units. They show optical modes lying at extremely low energy. This hints to a possible important role of these modes in the lattice dynamics even in the low temperature regime, where usually only acoustic phonons are expected to be populated. Furthermore,

the mixing between the latter and the low lying optical modes is present for all compounds.

The most striking difference between the three compounds is the increased number of bands in the low energy region of the vibrational spectra, passing from **1** to **3**. This effect is due to the increasing size of their unit cells, which in turn makes possible the formation of more low-energy

delocalized vibrations, involving, for instance, local molecular rotations and internal torsions. This feature is also highlighted by the vibrational density of states (DOS), reported in the right hand side of Figure 5. Indeed, the smallest density of states is computed for **1** while a much higher phonon density of states is computed for **3**. An intermediate result is computed for **2**.

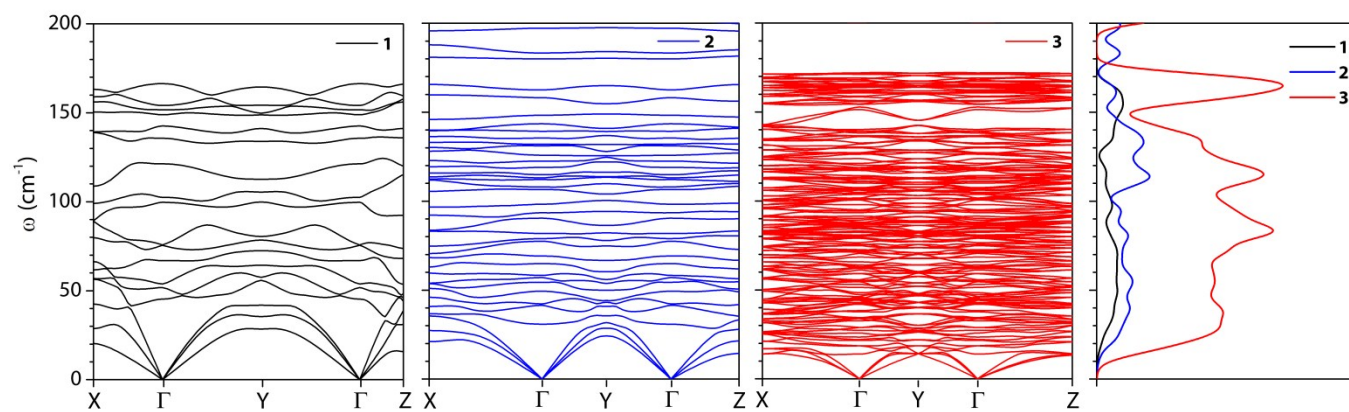


Figure 5. Dispersion curves for **1**, **2** and **3** (left) and normalized vibrational DOS (right).

A similar trend is also observed for the temperatures at which the three systems access to non-zero density of states: the lowest and the highest were found for **3** and **1**, respectively.

Along the same progression of the unit cell dimensions (*vide supra*), it is also possible to observe the reduction of the acoustic bands slope. This is in agreement with the dependence of this property with the inverse square root of the mass of the unit cell. Indeed, proceeding from **1** to **3**, the slope of the acoustic branch, which correlates to the speed of sound in the crystal, decreases and an increased efficiency in promoting relaxation is thus expected.

As already discussed, the spin-phonon bottleneck effect is related to the inefficiency of the crystal lattice to dissipate the phonons created during the spin relaxation process. Therefore, the possibility to observe deviation of the spin dynamics as a side effect of the spin-phonon bottleneck is directly related to the conductivity of the material where the spin is embedded in. According to the heat conductivity (k) formula obtained from the Boltzmann transport equation (BTE), equation(3),⁴³ each phonon (iq) in the system contributes to this property with three factors: its life-time τ_{iq} , its group velocity v and its specific heat C_v :

$$k_{\alpha\beta} = \sum_{iq} C_{v_{iq}} v_{iq}^{\alpha} v_{iq}^{\beta} \tau_{iq} \quad (3)$$

At low temperature, the k limiting factor is expected to be the lacking of heat carriers (phonons) and this feature is accounted by the specific heat. This assumption is also in agreement with the Stoneham model (equation 2), where the ratio of the spin and lattice specific heats gauges the effects on τ by the phonons relaxation time, suppressing them completely for

high lattice specific heat. When the latter condition does not apply, the crystal non-equilibrium features, such as the phonon life-time, become relevant also for the spin dynamics. It should also be noted that τ_{iq} itself would in principle contribute to reduce the lattice thermal conductivity. However, its effects in this respect are expected to become notable only at high temperatures, where the anharmonic phonon-phonon scattering processes take place. The specific heat of a given mode, with energy $\hbar\omega_{iq}$, vanishes at 0 K and starts increasing with T according to:

$$C_{v_{iq}} = k_B \left(\frac{\hbar\omega_{iq}}{2k_B T} \right)^2 \operatorname{cosech}^2 \left(\frac{\hbar\omega_{iq}}{2k_B T} \right) \quad (4)$$

According to eq. (3) and eq.(4), the higher the phonon density of states near or below a certain $k_B T$, the higher would be the value of C_v and k at that temperature and, therefore, the lower would be the chance to observe the spin-phonon bottleneck. For what concerns the three samples under study, **1** is expected to show a spin-phonon bottleneck effect up to higher temperatures with respect to **2** and **3**, due to the dramatic drop in the amount of accessible phonons at frequencies lower than 30 cm^{-1} (40 K), corresponding to the highest temperature at which the spin-phonon bottleneck has been observed for this compound. The same argument holds for the comparison between **2** and **3**, where the latter would be expected to show a spin-phonon bottleneck to a lesser extent, as it indeed does. The presented analysis is, of course, mainly based on simple statistic considerations since it does not take into account the coupling of the vibrational and the spin degrees of freedom, but only a larger or minor density of states accessible at low

temperature. A preliminary attempt to face this problem was reported by Moreno *et al.*⁴⁴

Conclusions

In the last couple of years, the investigation of spin dynamics of simple molecules by AC susceptometry has allowed to identify in the vanadyl unit one of the most promising candidates for a potential application as molecular based quantum bits.^{9, 10, 33} However, the present study points out that these slow relaxing systems exhibit a giant spin-phonon bottleneck and the relaxation times can vary over several order of magnitudes depending on the crystallites size. This evidences the need to carry out comparison of relaxation times obtained by different samples with special care. In particular, it is of absolute importance to separate effects coming from the electronic structure and those related to the exchange of energy with the thermal bath.

The investigation of a series of compounds exhibiting the same electronic properties but different peripheral group on the ligands has evidenced the key role played by the phonon spectrum on the magnetization dynamics, highlighting that smaller molecules exhibit a more pronounced spin-phonon bottleneck effect and in general a slower relaxation due to a higher velocity of acoustic phonons, as estimated from a combination of DFT and molecular dynamics approaches. Interestingly, similar comparative studies performed in frozen solution have not highlighted any significant trend.¹⁴

Though the concentrated samples investigated here are not expected to exhibit long coherence time, the possibility to evaporate them on surfaces makes this family of complexes extremely appealing to further investigate the spin dynamics, once these molecules are deposited on a substrate. Indeed the latter can influence not only electronic but also vibrational degrees of freedom of the molecular system, as evidenced in this work. The reduced efficiency of energy exchange from the spin system to the thermal bath could actually contribute to enhance the magnetic bistability, as observed for Ho atoms²⁰ or TbPc₂ SMMs⁴⁵ on MgO thin films, which constitute a very rigid lattice. In these experiments, performed in ultra-high vacuum conditions, the thermalisation of the spin systems occurs, in fact, through the substrate, whose rational choice could be an additional tool to control the molecular spin dynamics.

Experimental

General remarks

Acetylacetone (acac), dipivaloylmethane (dpm) and dibenzoylmethane (dbm) were purchased from Sigma-Aldrich.

Powder X-Ray crystallography

Wide-Angle Powder X-ray Diffraction (PXRD) patterns on polycrystalline samples were recorded on a *Bruker New D8 Advance DAVINCI* diffractometer in a $\vartheta - \vartheta$ configuration

equipped with a linear detector. The scans were collected within the range 5–40° (2 θ) using CuK α radiation ($\lambda = 1.5406 \text{ \AA}$). The simulated patterns were generated from the atomic coordinates of the single crystal structure solutions using the Mercury CSD 3.3 program⁴⁶ (copyright CCDC, <http://www.ccdc.cam.ac.uk/mercury/>) using a FWHM (full width at half maximum) of 0.15 and a 2 θ step of 0.025.

Electron paramagnetic resonance (EPR) analysis

X-Band EPR spectra were recorded on a Bruker Elexsys E500 spectrometer equipped with a SHQ cavity ($\nu = 9.392 \text{ GHz}$). Low temperature (50 K) needed to freeze the measured solutions (1 mM, 2:3 toluene: CH₂Cl₂) was obtained using an Oxford Instruments ESR900 continuous flow helium cryostat.

Magnetic measurements

Alternate current (AC) susceptibility measurements were performed in the temperature range 1.8–40 K with applied magnetic fields up to 8.8 T on polycrystalline samples of compounds **1-3**, by using a *Quantum Design Physical Property Measurement System (PPMS)* equipped with a AC susceptometer operating in the 10 Hz–10 kHz frequency range and a *Quantum Design Magnetic Property Measurement System (MPMS)* equipped with a *Superconducting Quantum Interference Device (SQUID)* AC susceptometer operating in the 0.1 Hz–1 kHz frequency range at the same gas exchange pressure (ca. 10 Torr) for all measurements. All samples were measured wrapped in teflon. The well crushed (c) samples were also pressed in a pellet. Susceptibility and magnetic data were corrected for the sample holder previously measured using the same conditions and for the diamagnetic contributions as deduced by using Pascal's constant tables (Figure S7-S16).⁴⁷

Force Field parametrization

Force field parameters for the three molecules have been derived following the procedure outlined by Ryde⁴⁸ and exploiting the software Hess2FF.⁴⁹ This approach requires the calculation of the hessian matrix for the three isolated molecules in order to map their eigenvalues and eigenvectors on the chosen intra-molecular force field energy representation. In this work, the energy has been chose according to the GAFF recipe,⁵⁰ except for the choice of completely screening the non-bonded 1-4 interactions (they have been set to zero) in order to minimize the known shortcoming of the parametrization method.⁴⁸ In this framework, all the parameters related to internal degrees of freedom have been optimized and no use of the GAFF library has been made for the intra-molecular interactions. On the other hand, the non-bonded part of the force field, composed by vdW and coulomb interactions, has been set up with the original GAFF's Lennard Jones parameters and with RESP charges. The assessment of the FF quality has been made on the basis of its ability to reproduce structural features of both isolated molecules and their crystalline cells. While the isolated DFT calculations used as basis for the FF mapping offer a straightforward way to rationalize the quality of the mapping

itself, another set of ab initio reference calculations for the periodic crystals must be provided. This second reference has been produced through the optimization of the unit cells for **1**, **2** and **3** with a periodic boundary condition based DFT software (pDFT). A good overall agreement has been obtained between FF, DFT, pDFT and experimental parameters. The details of these tests are listed and further discussed in the ESI.

All aforementioned optimization, hessian and RESP charges calculations on the isolated molecules have been carried out with the software Gaussian09⁵¹ at the DFT level of theory. All the elements have been described with a 6-31G* basis set and the PBE⁵² functional. pDFT calculations have been executed on the molecules unit cell with the CP2K software⁵³, employing the PBE functional with the DZVP-MOLOPT basis set and a plane waves cut-off of 500 Ry, for all the elements. In all DFT simulation protocols Grimme's D3 vdW correction scheme has been employed⁵⁴.

Lattice dynamics

Crystal properties calculations have been carried out with an home-made software for the lattice dynamics part and with lammps molecular dynamics package⁵⁵ for what concerns crystal cells optimization and force calculations. Forces have been calculated employing Ewald summations on the reciprocal space with an accuracy of 1.0×10^8 for the long-range part of both electrostatic and dispersion interactions.

The dynamical matrices of the three molecules supercells have been computed by force fields through lammps. The supercell of **1** and **2** has been chosen as $3 \times 3 \times 3$ times the primitive cell (two molecules each), while the supercell of **3**, due to the larger amount of molecules contained, has been modelled as $2 \times 2 \times 2$ times the primitive cell (eight molecules). The three supercells have been optimized with lammps through a thermal annealing procedure with a final optimization at 0 K of both atomic positions and cell parameters. The optimized supercells have then been used to evaluate lattice properties by perturbation theory.⁵⁶ The real space dynamical matrix elements are defined as

$$f_{st}(ki, k'j) = \frac{\partial^2 E}{\partial x_{kis} \partial x_{k'jt}} \quad (5)$$

The indexes k and k' run over the cells inside the supercell, i and j run over the atoms inside the specific cell while s and t run over the three cartesian spatial coordinates. The calculation of $f_{st}(ki, k'j)$ has been done by numerical differentiation, displacing each atoms in the primitive cell by ± 0.01 Å along the three spatial directions. Convergence of the results with respect to the differentiation step has been checked. The real space force constants have then been used to build the dynamical matrix

$$D_{st}(ij, q) = \frac{1}{\sqrt{m_i m_j}} \sum_{k'} f_{st}(ki, k'j) \exp[iq \cdot (r(k') - r(k))] \quad (6)$$

where m are the masses of the atoms in the $k|k'$ cell inside the considered supercell and q represents a vector in the reciprocal primitive lattice. Finally, $r(k)-r(k')$ represents the distance between the primitive cell k and the considered cell k' in the supercell.

The vibrational density of states (DOS) is defined as

$$DOS(\omega) = \frac{1}{N_q} \sum_{\alpha q} \delta(\omega - \omega_{\alpha q}) \quad (7)$$

where N_q is the number of q -points in the reciprocal space and $\omega_{\alpha q}$ is the α eigenvalue obtained through diagonalization of the dynamical matrix $D(q)$.

The DOS have been obtained integrating the Brillouin zone with a $8 \times 8 \times 8$ regular mesh of points in the crystals reciprocal space. A normalized Gaussian broadening, with σ of 5 cm^{-1} , has also been applied to all frequencies.

Acknowledgements

Dr. S. Ciattini (CRIST, Univ. of Florence) is acknowledged for assistance in microtomography experiments and Dr. M. Perfetti for useful discussion. We acknowledge the financial support of European Research Council (ERC) through AdG MolNanoMaS (267746), Italian MIUR through the project Futuro in Ricerca 2012 (RBFR12RPD1), and Fondazione Ente Cassa di Risparmio di Firenze.

Notes and references

1. D. Gatteschi, R. Sessoli and J. Villain, *Molecular nanomagnets*, Oxford University Press, Oxford, UK, 2006.
2. J. Dreiser, *J. Phys. Condens. Matter*, 2015, **27**, 183203.
3. A. Cornia and M. Mannini, *Structure and Bonding*, 2014, **150**, 1-38.
4. M. L. Perrin, E. Burzurí and H. S. J. van der Zant, *Chem. Soc. Rev.*, 2015, **44**, 902-919.
5. M. Urdampilleta, S. Klyatskaya, J. P. Cleuziou, M. Ruben and W. Wernsdorfer, *Nat. Mater.*, 2011, **10**, 502-506.
6. E. Burzurí, Y. Yamamoto, M. Warnock, X. Zhong, K. Park, A. Cornia and H. S. J. van der Zant, *Nano Lett.*, 2014, **14**, 3191-3196.
7. A. Ardavan, O. Rival, J. J. L. Morton, S. J. Blundell, A. M. Tyryshkin, G. A. Timco and R. E. P. Winpenny, *Phys. Rev. Lett.*, 2007, **98**, 057201.
8. K. Bader, D. Dengler, S. Lenz, B. Endeward, S.-D. Jiang, P. Neugebauer and J. van Slageren, *Nat. Commun.*, 2014, **5**, 5304.
9. M. Atzori, L. Tesi, E. Morra, M. Chiesa, L. Sorace and R. Sessoli, *J. Am. Chem. Soc.*, 2016, **138**, 2154-2157.
10. L. Tesi, E. Lucaccini, I. Cimatti, M. Perfetti, M. Mannini, M. Atzori, E. Morra, M. Chiesa, A. Caneschi, L. Sorace and R. Sessoli, *Chem. Sci.*, 2016, **7**, 2074-2083.
11. M. Warner, S. Din, I. S. Tupitsyn, G. W. Morley, A. M. Stoneham, J. A. Gardener, Z. Wu, A. J. Fisher, S. Heutz, C. W. M. Kay and G. Aeppli, *Nature*, 2013, **503**, 504-508.

12. C. J. Wedge, G. A. Timco, E. T. Spielberg, R. E. George, F. Tuna, S. Rigby, E. J. L. McInnes, R. E. P. Winpenny, S. J. Blundell and A. Ardavan, *Phys. Rev. Lett.*, 2012, **108**, 107204.
13. J. M. Zadrozny, J. Niklas, O. G. Poluektov and D. E. Freedman, *J. Am. Chem. Soc.*, 2014, **136**, 15841-15844.
14. J. M. Zadrozny, J. Niklas, O. G. Poluektov and D. E. Freedman, *ACS Central Sci.*, 2015, **1**, 488-492.
15. M. A. Nielsen and I. L. Chuang, *Quantum Computation and Quantum Information*, Cambridge University Press, Cambridge, 2000.
16. J. Ferrando-Soria, E. M. Pineda, A. Chiesa, A. Fernandez, S. A. Magee, S. Carretta, P. Santini, I. J. Vitorica-Yrezabal, F. Tuna, G. A. Timco, E. J. L. McInnes and R. E. P. Winpenny, *Nat. Commun.*, 2016, **7**, 11377.
17. K. Bader, M. Winkler and J. van Slageren, *Chem. Commun.*, 2016, **52**, 3623-3626.
18. A. Morello, *Nat. Mater.*, 2015, **14**, 135-136.
19. A. Morello, *Nanotechnology*, 2015, **26**, 502501.
20. F. Donati, S. Rusponi, S. Stepanow, C. Wäckerlin, A. Singha, L. Persichetti, R. Baltic, K. Diller, F. Patthey, E. Fernandes, J. Dreiser, Ž. Šljivančanin, K. Kummer, C. Nistor, P. Gambardella and H. Brune, *Science*, 2016, **352**, 318-321.
21. J. H. van Vleck, *Phys. Rev.*, 1941, **59**, 724-729.
22. K. S. Pedersen, J. Dreiser, H. Weihe, R. Sibille, H. V. Johannesen, M. A. Sørensen, B. E. Nielsen, M. Sigrist, H. Mutka, S. Rols, J. Bendix and a. S. Piligkos, *Inorg. Chem.*, 2015, **54**, 7600-7606.
23. A. M. Stoneham, *Proc. Phys. Soc.*, 1965, **86**, 1163.
24. K. J. Standley and R. A. Vaughan, *Electron Spin Relaxation Phenomena in Solids*, Plenum Press, New York, 1969.
25. I. Chiorescu, W. Wernsdorfer, A. Muller, H. Bogge and B. Barbara, *Phys. Rev. Lett.*, 2000, **84**, 3454-3457.
26. K. Petukhov, S. Bahr, W. Wernsdorfer, A.-L. Barra, and V. Mosser, *Phys. Rev. B* 2007, **75**, 064408.
27. G. de Loubens, D. A. Garanin, C. C. Beedle, D. N. Hendrickson and A. D. Kent, *Europhys. Lett.*, 2008, **83**, 37006.
28. O. Waldmann, R. Koch, S. Schromm, P. Müller, I. Bernt and R. W. Saalfrank, *Phys. Rev. Lett.*, 2002, **89**, 246401.
29. D. M. Murphy, I. A. Fallis, R. D. Farley, R. J. Tucker, K. L. Avery, D. J. Willock, *PCCP*, 2002, **4**, 4937-4943.
30. E. Shuter, S. J. Rettig, C. Orvig, *Acta Crystallogr., Sect. C: Cryst. Struct. Commun.*, 1995, **51**, 12.
31. M. Mohamadi, S. Y. Ebrahimipour, M. Torkzadeh-Mahani, S. Foro, A. Akbari, *RSC Advances* 2015, **5**, 101063.
32. M. A. K. Ahmed, H. Fjellvåg, A. Kjekshus and B. Klewe, *Z. Anorg. Allg. Chem.*, 2004, **630**, 2311-2318.
33. M. Atzori, E. Morra, L. Tesi, M. Chiesa, L. Sorace and R. Sessoli, *Submitted for publication*.
34. S. Stoll and A. Schweiger, *J. Magn. Reson.*, 2006, **178**, 42-55.
35. A. J. Fielding, D. B. Back, M. Engler, B. Baruah, D. C. Crans, G. R. Eaton and S. S. Eaton, *ACS Symp. Ser.*, 2007, **974**, 364-375.
36. J. P. Fackler, J. D. Levy and J. A. Smith, *J. Am. Chem. Soc.*, 1972, **94**, 2436-2445.
37. A. C. De Vroomen, E. E. Lijphart, D. Y. H. Prins, J. Marks and N. J. Poulis, *Physica*, 1972, **61**, 241-249.
38. J. H. van Vleck, *Phys. Rev.*, 1940, **57**, 426-447.
39. S. Gómez-Coca, A. Urtizbera, E. Cremades, P. G. Alonso, A. Camón, E. Ruiz and F. Luis, *Nat. Commun.*, 2014, **5**, 4300.
40. A. Abragam and B. Bleaney, *Electron Paramagnetic Resonance of Transition Ions*, Dover, New York, 1986.
41. K. N. Shrivastava, *Phys. St. Solidi B*, 1983, **117**, 437-458.
42. J.-L. Du, G. R. Eaton and S. S. Eaton, *J. Magn. Reson. A*, 1996, **119**, 240-246.
43. A. J. H. McGaughey and M. Kaviani, *Phys. Rev. B*, 2004, **69**, 094303.
44. L. E. Moreno, N. Suaud and A. G. Arino, *arXiv:1512.05690*, 2015.
45. C. Wäckerlin, F. Donati, A. Singha, R. Baltic, S. Rusponi, K. Diller, F. Patthey, M. Pivetta, Y. Lan, S. Klyatskaya, M. Ruben, H. Brune and J. Dreiser, *Adv. Mater.*, 2016, **28**, 5195-5199.
46. C. F. Macrae, P. R. Edgington, P. McCabe, E. Pidcock, G. P. Shields, R. Taylor, M. Towler and J. van de Streek, *J. Appl. Crystallogr.*, 2006, **39**, 453-457.
47. G. A. Bain and J. F. Berry, *J. Chem. Educ.*, 2008, **85**, 532.
48. L. H. Hu. and U. Ryde, *J. Chem. Theory Comput.*, 2011, **7**, 2452-2463.
49. P. Rydberg, L. Olsen, P. -O. Norrby and U. Ryde, *J. Chem. Theory Comput.*, 2007, **3**, 1765-1773.
50. J. M. Wang, R. M. Wolf, J. W. Caldwell and P. A. Kollman, *J. Chem. Comput.*, 2004, **25**, 1157-1174.
51. M. J. Frisch, G. W. Trucks, H. B. Schlegel, G. E. Scuseria, M. A. Robb, J. R. Cheeseman, G. Scalmani, V. Barone, B. Mennucci, G. A. Petersson, H. Nakatsuji, M. Caricato, X. Li, H. P. Hratchian, A. F. Izmaylov, J. Bloino, G. Zheng, J. L. Sonnenberg, M. Hada, M. Ehara, K. Toyota, R. Fukuda, J. Hasegawa, M. Ishida, T. Nakajima, Y. Honda, O. Kitao, H. Nakai, T. Vreven, J. A. Montgomery, Jr., J. E. Peralta, F. Ogliaro, M. Bearpark, J. J. Heyd, E. Brothers, K. N. Kudin, V. N. Staroverov, R. Kobayashi, J. Normand, K. Raghavachari, A. Rendell, J. C. Burant, S. S. Iyengar, J. Tomasi, M. Cossi, N. Rega, J. M. Millam, M. Klene, J. E. Knox, J. B. Cross, V. Bakken, C. Adamo, J. Jaramillo, R. Gomperts, R. E. Stratmann, O. Yazyev, A. J. Austin, R. Cammi, C. Pomelli, J. W. Ochterski, R. L. Martin, K. Morokuma, V. G. Zakrzewski, G. A. Voth, P. Salvador, J. J. Dannenberg, S. Dapprich, A. D. Daniels, Ö. Farkas, J. B. Foresman, J. V. Ortiz, J. Cioslowski, and D. J. Fox, *Gaussian 09, Revision E.01*, 2009.
52. A. Becke, *J. Chem. Phys.*, 1993, **98**, 5648-5652.
53. J. Hutter, M. Iannuzzi, F. Schiffrmann and J. VandeVondele, *Wiley Interdisciplinary Reviews: Computat. Mol. Sci.*, 2014, **4**, 15-25.
54. S. Grimme, J. Antony, S. Ehrlich and H. Krieg, *J. Chem. Phys.*, 2010, **132**, 154104.
55. S. Plimpton, *J. Comput. Phys.*, 1995, **117**, 1-19.
56. S. Califano, V. Schettino and N. Neto, *Lattice Dynamics of Molecular Crystals*, Springer, Berlin, 1981.

Table of Content entry

The smaller the ligand the slower is the low temperature magnetization dynamics of crystals of vanadyl complexes

